Available online at www.sciencedirect.com
SCIENCE DIRECT®
Journal of Power Sources 135 (2004) 255–261
JOURNAL OF POWER SOURCES
www.elsevier.com/locate/jpowsour

In situ electrochemical impedance spectroscopy to investigate negative electrode of lithium-ion rechargeable batteries

Masayuki Itagaki [a,*], Nao Kobari [a], Sachiko Yotsuda [a], Kunihiro Watanabe [a], Shinichi Kinoshita [b], Makoto Ue [b]

[a] *Department of Pure and Applied Chemistry, Faculty of Science and Technology, Tokyo University of Science, Noda, Chiba 278-8510, Japan*
[b] *Mitsubishi Chemical Group, Science & Technology Research Center, 8-3-1, Chuo, Ami, Inashiki Ibaraki 300-0332, Japan*

Received 10 December 2003; accepted 1 April 2004

Abstract

The in situ electrochemical impedance spectroscopy (in situ EIS) in which the impedance spectra are measured simultaneously with the charge (intercalation)—discharge (deintercalation) sequence of lithium-ion rechargeable batteries has been developed. This method was applied to the investigation of the graphite electrode of lithium-ion rechargeable batteries. The resistance R_{sei} for lithium-ion permeation in the solid electrolyte interphase (SEI) film were determined, and the formation mechanisms of SEI was discussed. Moreover, the role of vinylene carbonate (VC) as an additive to $LiPF_6$–ethylene carbonate/ethyl methyl carbonate electrolyte solution was investigated. It was clarified that R_{sei} decreases by the addition of VC, indicating the formation of a high quality SEI film.

Keywords: Electrochemical impedance; Graphite electrode; Lithium-ion rechargeable batteries; Vinylene carbonate

1. Introduction

Since graphite can be transformed to the graphite intercalation compounds (GIC) by the intercalation of various kinds of atoms, the graphite has been used as a negative electrode of lithium-ion rechargeable batteries [1]. It is well known that a stable film is formed on the graphite electrode in ethylene carbonate (EC) electrolyte solution. This film protects the electrolyte solution from its further decomposition and it is a lithium-ion conductive material [2]. This film is formed by the decomposition of the electrolyte solution during the first cycle charge and called as a solid electrolyte interphase (SEI). It is known that the SEI has multi-layer structure composed of inorganic components like LiF, Li_2O and Li_2CO_3 and organic species (polymers) like $ROCO_2Li$ [3]. Beside, it was reported that the intercalation of solvated lithium-ions into graphite was the first step to form SEI on the graphite electrode and that the decomposition products by the reduction of co-intercalated electrolyte solution became the SEI [4]. Inaba and co-workers [5–8] observed a highly oriented pyrolytic graphite (HOPG) surface in propylene carbonate (PC) and EC electrolyte solutions by a scanning tunneling microscope (STM), and stated in the reference [6] that the intercalation of solvated lithium-ions corresponded to the initial stage of the solvent decomposition and subsequent film formation processes.

It is possible to obtain the electrochemical parameters inside the battery without its destruction by the application of an electrochemical impedance spectroscopy (EIS). Therefore, EIS has been used to analyze the negative graphite electrode reaction of the lithium-ion rechargeable batteries [9–12]. Osaka et al. [13] investigated the lithium electrode in PC electrolyte solution during charge and discharge cycles by in situ electrochemical impedance spectroscopy (in situ EIS). The frequency range of their measurements [13] was above 10 Hz because the electrode reaction in secondary batteries does not satisfy the time stability during the charge and discharge cycles and the low frequency components of impedance contains significant errors due to the time variation. The time stability of the electrode means no variation of electrode reaction rate during the measurement of the impedance spectrum, and it is required in the measurement of general EIS. Stoynov et al. [14] proposed the method to compensate the deviation of low frequency components of the impedance without time stability by using three-dimensional (3D) complex plot, whose axes are real,

* Corresponding author. Tel.: +81 4 7122 9492; fax: +81 4 7123 9890.
E-mail address: itagaki@rs.noda.tus.ac.jp (M. Itagaki).

0378-7753/$ – see front matter © 2004 Elsevier B.V. All rights reserved.
doi:10.1016/j.jpowsour.2004.04.004

imaginary parts and time. Beside, Itagaki et al. [15] applied this method to the investigation of anodic dissolution mechanisms of metal. Stoynov et al. [16] used in situ EIS with this compensation method [14] for the investigation of lead acid battery. In the present paper, the suitable impedances for the negative electrode of lithium-ion rechargeable batteries during charge and discharge cycles are obtained by the above-mentioned compensation, and the intercalation of lithium-ion and the formation mechanism of SEI film are analyzed. In all impedance analysis on the negative electrode reported until now, the charge–discharge was stopped to measure the impedance spectrum [9]. The purpose of the present paper is to develop the in situ EIS to measure the impedance spectra simultaneously with the charge and discharge cycles.

2. Experimental

2.1. The electrochemical cell

The cell used for the experiments is shown in Fig. 1. The graphite working electrode (WE) (Mitsubishi Power Graphite (MPG), Mitsubishi Chemical Corp.) (1 cm × 0.4 cm) was prepared by bonding graphite powder (11.7 mg cm^{-2}) onto a copper foil as a current collector, and by successively pressing by 50 MPa for 1 min. A lithium foil was used as the counter electrode (CE) and a lithium wire was used as the reference electrode (RE). The potential of WE in this paper is represented as basis of the potential of RE. A polyethylene (PE) filter as the separator was sandwiched between WE and CE. In order to prevent the deformation of WE due to the volume change by electrolysis, the WE and CE were fixed with nickel plates. The electrolyte solution was a mixture of an ethylene carbonate (EC) and an ethyl methyl carbonate (EMC) (3:7 by vol.) containing 1 M $LiPF_6$ with or without 2 wt.% vinylene carbonate (VC) (Sol-Rite, Mitsubishi Chemical Corp.). All experiments were carried out at room temperature (25 °C) in a dry argon atmosphere.

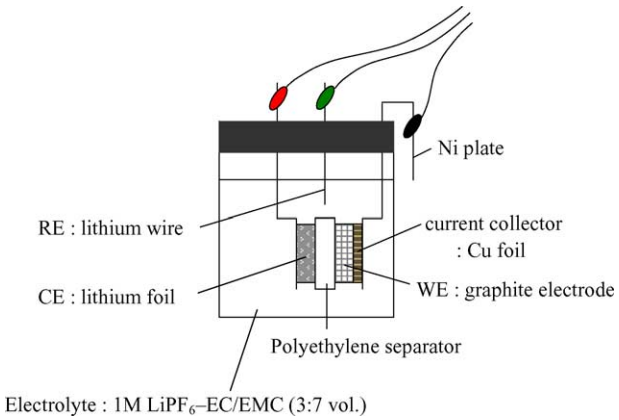

Fig. 1. The electrochemical cell to investigate the reaction at electrolyte–graphite interface.

2.2. Charge–discharge curves and simultaneous impedance measurements

During the measurements of the charge–discharge curves at the DC current density of 0.2 mA cm^{-2}, the impedance spectra were measured successively by superimposing the small AC current on the DC current. The amplitude of the AC current was decided to make the AC component of potential response smaller than 5 mV. The impedance measurement was carried out in a frequency range from 10 mHz to 10 kHz, and started from high frequency toward low frequency in the logarithmic scan. In the early period of charge and the end of discharge, the impedance measurements were carried out in a frequency range from 100 mHz to 10 kHz to decrease the measurement time. In the present paper, the charge is defined as the intercalation of lithium into the graphite electrode, and the discharge is defined as the deintercalation of lithium from the graphite electrode. The experimental set-up consisted of a potentiostat (Hokuto Denko, HA501G) and a frequency response analyzer (FRA) (NF block, 5020) controlled by a personal computer (IBM, ThinkPad A22m) through GP–IB interface. In order to compensate the impedance spectrum deviated by the variation of reaction resistance due to charge and discharge, the impedance spectra were measured successively and plotted on the 3D complex diagram, which has a time axis. The plots were connected by the spline under tension function at each frequency (Fig. 2a) [15]. In Fig. 2b, the cross section of 3D impedance shell perpendicular to the time axis gives the instantaneous impedance at an arbitrary time presented in Fig. 2c [15]. The impedance and the parameters obtained by the impedance were represented by the values per the surface area (0.4 cm^2) of the working electrode.

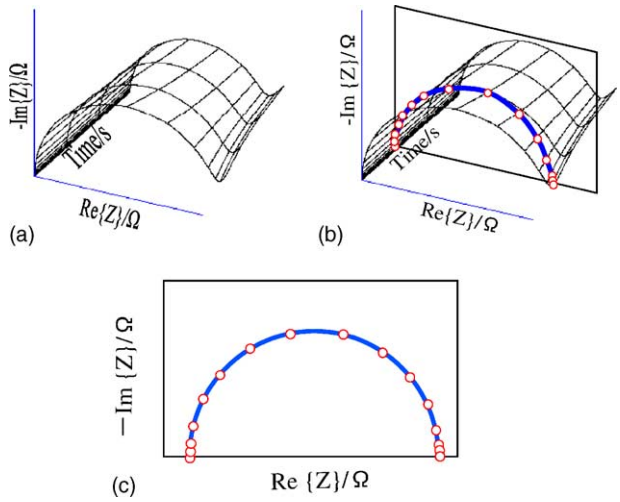

Fig. 2. (a) Scheme of 3D complex plot of impedance, (b) the cross section of 3D impedance shell perpendicular to time axis, (c) the instantaneous impedance obtained from the cross section.

3. Results and discussion

3.1. Electrochemical measurement for graphite electrode in 1 M $LiPF_6$–EC/EMC electrolyte solution

3D complex plots of the electrochemical impedance during the first and second charge–discharge cycles are shown in Fig. 3. The results in the initial and end periods during the charge are shown in Fig. 3(a1) and (a2), respectively. On the other hand, the results in the initial and end periods during the discharge are shown in Fig. 3(b1) and (b2), respectively. Since the impedance spectrum changes significantly depending on the time in Fig. 3(a1), the time axis and the real number axis were exchanged to visualize it clearly. The diameter of capacitive loop takes a large value at the early period of the first cycle charge and decreases abruptly with the charge time. In Fig. 3(a2), the impedance spectrum shows not only the capacitive loop but also the inductive loop, and does not show the apparent time variation. The impedance at the initial period of the second cycle charge in Fig. 3(c1) is remarkably different from that of the first cycle charge in Fig. 3(a1), namely, the abrupt decrease of impedance is not observed in Fig. 3(c1). The impedance spectrum at the initial period of the first cycle discharge in Fig. 3(b1) shows the both capacitive and inductive loops, and the diameters of loops decrease with the discharge time. In Fig. 3(b2), the impedance shows two capacitive loops, and does not show apparent time variation. The impedance in the second cycle discharge in Fig. 3(d1) and (d2) has the almost same feature as the results in Fig. 3(b1) and (b2).

Fig. 4 shows the potential–capacity curve of the graphite electrode in EC/EMC electrolyte solution containing 1 M $LiPF_6$ and the impedance, which were determined simultaneously. The lithium-ion intercalation occurs randomly into the graphite electrode in the early period of the charge in the potential region above 0.2 V. It was reported that SEI film formation takes place in this potential region [13]. The GIC is generated in the potential domain below 0.2 V. The impedance presented in Fig. 4 was the instantaneous impedance obtained from the cross section of 3D impedance at an arbitrary time in Fig. 3. The current imposed for the potential–capacity curve in Fig. 4 consists of DC and small AC components. The potential–capacity curve in Fig. 4 agrees completely with the curve that was measured by imposing only DC current. This agreement was also confirmed in the potential–capacity curves during all charge and discharge cycles. This agreement indicates no influence of small AC current superimposition on potential–capacity curve. In Fig. 4, the impedance shows two capacitive loops at early period in the first charge cycle. The high frequency loop in the impedance spectra is related to the time constant of lithium-ion permeation through SEI film. The low frequency loop is related to the time constant of charge-transfer resistance and electrical double layer capacitance on the graphite particle surface [9]. With the furthermore charge, the inductive loop appears in the low frequency range. In the previous papers concerning EIS study on the graphite negative electrode [9,11,12], its inductive behavior has never been discussed. Because the impedance spectra are determined simultaneously with charge and discharge cycle, the impedance regarding to dynamic electrode condition can be obtained in the present paper. For example, the inductive loop is also observed in the active dissolution of metals [17,18]. In the literatures [17] and [18], the inductive behavior originates from the decrease of the reaction resistance by the catalysts formed on the electrode. Since the intercalation of lithium-ion could be concerned with the electrode resistance in the case of graphite electrode, the electrochemical behavior of the intercalation site could be discussed on the basis of the inductive loop. Graphite is a typical layered substance that consists of hexagonal sheets of sp^2–carbon atoms (graphene layers). The graphene layers are weakly bonded together by van der Waals forces as an $A \cdot B \cdot A \cdot B \cdots$ stacking sequence along the *c*-axis. Lithium-ions are intercalated between the graphene layers to form GIC [19]. The distance between graphene layers is expanded by the intercalation of the lithium-ion into each interlayer, and the resistance of the intercalation of the following lithium-ions became small. Therefore, it can be considered that the above-mentioned inductive period yields the inductive loop in the Nyquist plot of the impedance.

3.2. Discussion on the parameters obtained from the impedance of graphite electrode in 1 M $LiPF_6$–EC/EMC

The typical impedance of graphite electrode in 1 M $LiPF_6$–EC/EMC (3:7 by vol.) and an equivalent circuit used to analyze the electrochemical process for the lithium-ion intercalation into the graphite electrode are shown in Fig. 5. In Fig. 5, R_{sol} represents the electrolyte resistance, R_{sei} and C_{sei} are the resistance and capacitance of the SEI film, respectively, and R_{ct} and C_{dl} are the charge-transfer resistance and double-layer capacitance on the graphite particle surface, respectively. Zhang et al. [9] was taking into consideration the Warburg impedance by the semi-infinite diffusion of the lithium-ions in graphite electrode. Chung et al. [11] used the equivalent circuit in which the time constant of the SEI film is divided into two. Wang et al. [12] divided the time constant of the SEI film into three. However, since the more than two capacitive loops cannot be distinguished from the impedance spectra of graphite electrode in 1 M $LiPF_6$–EC/EMC (3:7 by vol.) in the present results, the equivalent circuit in Fig. 5 was selected to examine the experimental results in the present paper.

The potential change against the capacity of graphite electrode during the first and second charge–discharge cycles at 0.2 mA cm^{-2} is shown in Fig. 6a. Electrolyte solution is a 1 M $LiPF_6$–EC/EMC (3:7 by vol.). The potential in the first cycle charge decreases rapidly from open circuit potential (about 3 V) to 0.2 V, and then a potential plateau appears less noble potential than 0.2 V. The intercalation of lithium-ion advances with the formation of

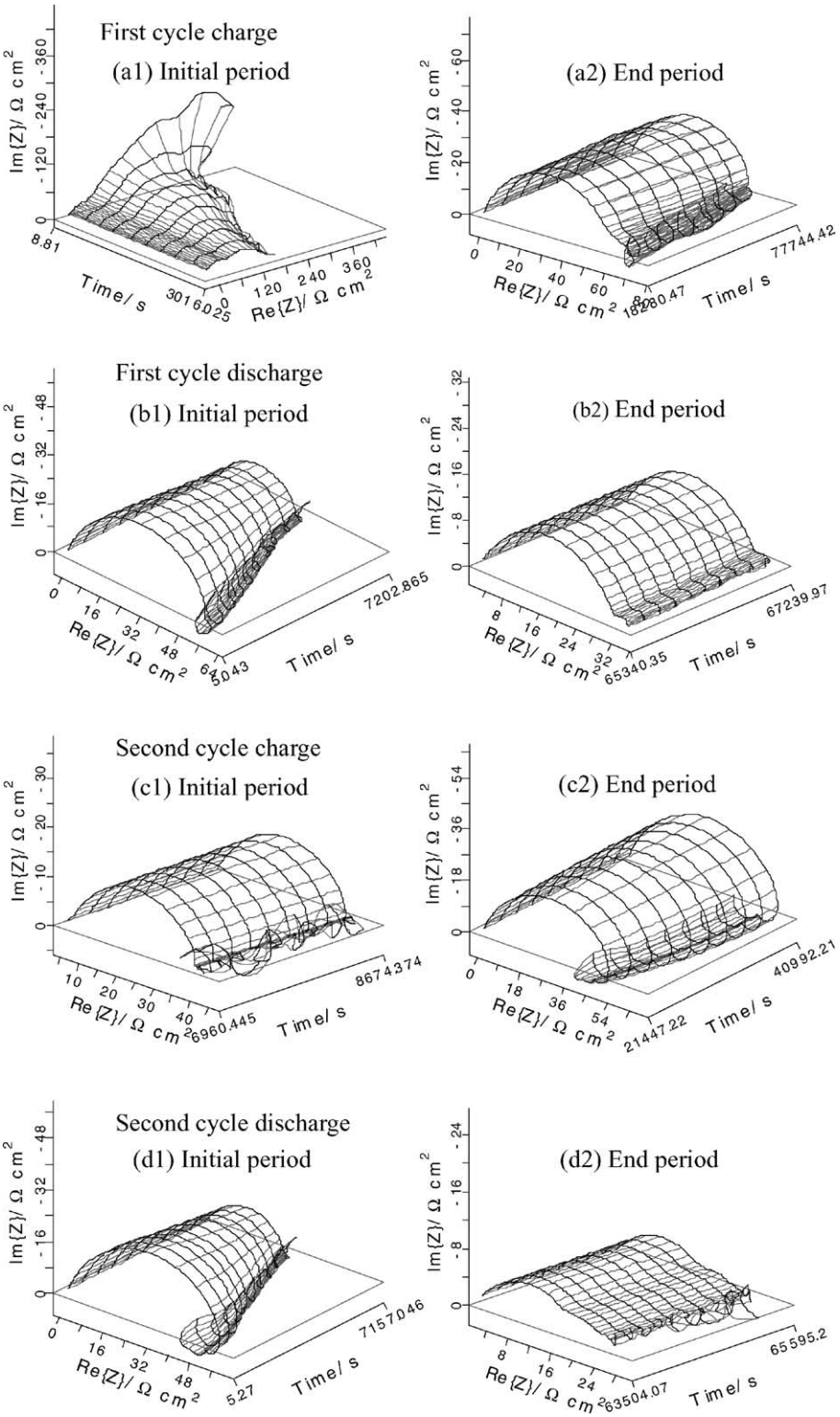

Fig. 3. 3D complex plots of electrochemical impedance during the first and second charge–discharge cycles.

GIC in this potential plateau. Moreover, the potential rises gradually to about 0.25 V in the first cycle discharge, and the potential rises rapidly to complete the discharge. It was calculated from Fig. 6a that the coulombic efficiency of delithiation during the first cycle is 90% and irreversible capacity is 10%. In the second cycle, the irreversible capacity decreases and the coulombic efficiency becomes 96%. It was reported that the main cause of this irreversible capacity

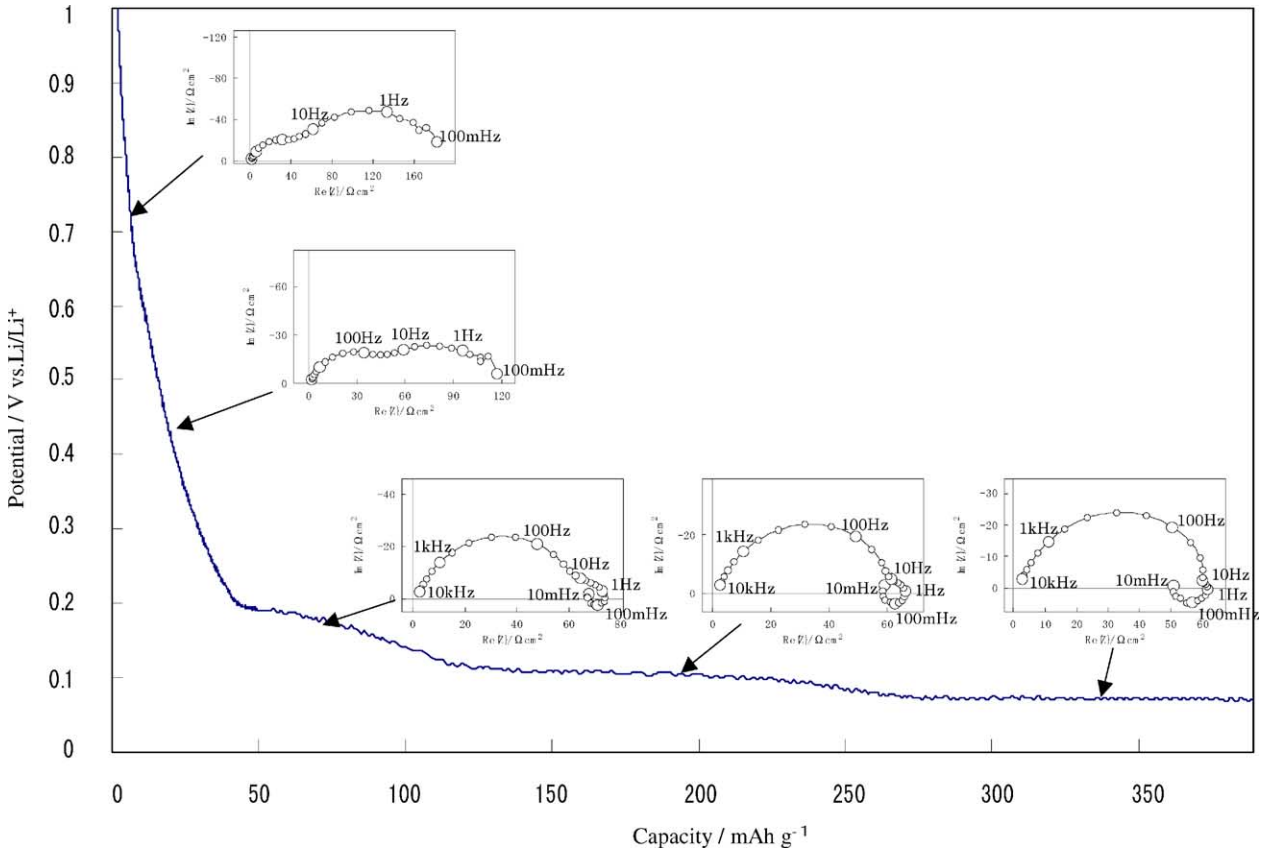

Fig. 4. Potential–capacity curve of the graphite electrode in 1 M $LiPF_6$–EC/EMC (3:7 by vol.) in the first cycle charge and the impedances which were determined simultaneously. The current density is 0.2 mA cm^{-2}.

was the formation of SEI film on the graphite electrode [20–24].

The parameters (R_{sol}, R_{sei}, R_{ct}, C_{sei}, and C_{dl}) were determined by the curve fitting using Zview software (Solartron) with the equivalent circuit shown in Fig. 5. The sequences of R_{sei} and R_{ct} are focused and discussed in this section. Fig. 6b shows the plots of R_{sei} against the capacity, and R_{sei} increases slightly in the early period in the first cycle charge. Zhang et al. [9] previously observed this phenomenon and stated

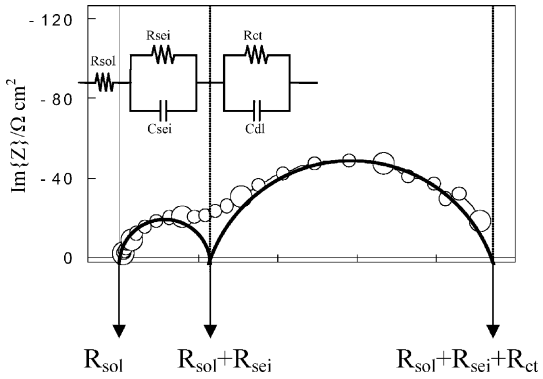

Fig. 5. The typical electrochemical impedance of graphite electrode in 1 M $LiPF_6$–EC/EMC (3:7 by vol.) and the equivalent circuit. The plots were the instantaneous impedance at 2156 s during the first cycle galvanostatic (0.2 mA cm^{-2}) charge.

that the loose and resistive SEI film was formed on graphite electrode above 0.25 V in the first cycle charge. Furthermore in the first cycle charge, R_{sei} decreases at 0 mAh g^{-1} and this result is also in agreement with the reference [9], which reported that the protective and conductive SEI film was formed below 0.25 V in the first cycle charge. In the first and second discharge cycles, R_{sei} decreases obviously at the large value of the capacity. Zhang et al. [9] presented the R_{sei} against the electrode potential, and reported that the R_{sei} increases and decreases with the charge and discharge, respectively, after second cycle. The hysterisis of R_{sei} during the charge and discharge cycle will be discussed in the next section.

In Fig. 6c, the R_{ct} decreases abruptly in the initial period and decreases gradually above 0 mAh g^{-1} during the first cycle charge. This behavior originates from that the area of SEI film/graphite interface increases by the co-intercalation of the electrolyte solution in the initial period.

3.3. Discussion on the parameters obtained from the impedance of graphite electrode in the electrolyte solution involving 2 wt.% vinylene carbonate (VC)

It has been clarified recently that vinylene carbonate (VC) is a significant additive to improve the ability of the negative electrode of lithium-ion rechargeable batteries. Aur-

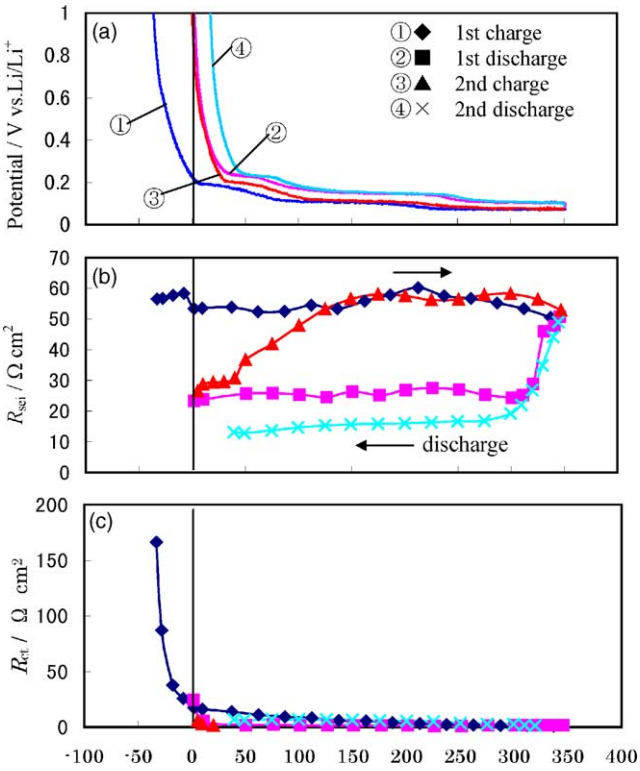

Fig. 6. The variations of the electrode potential and some parameters obtained from the experimental impedance of graphite electrode during the first and second charge–discharge cycles at 0.2 mA cm^{-2}. Electrolyte solution was a 1 M $LiPF_6$–EC/EMC (3:7 by vol.) solution.

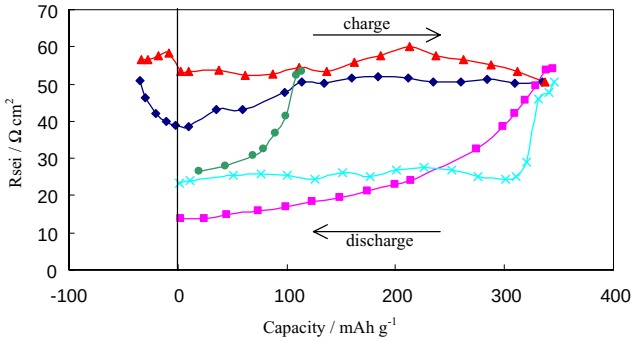

Fig. 7. The plots of R_{sei} of graphite electrode vs. the capacity during the first charge–discharge cycle at 0.2 mA cm^{-2}. Electrolyte solutions were a 1 M $LiPF_6$–EC/EMC (3:7 by vol.) without VC ((▲) during charge, (×) during discharge) and with 2 wt.% VC ((◆) during charge, (■) during discharge). The plots (●) denote the R_{sei} during discharge when the first cycle charge was turned to the discharge at 110 mAh g^{-1}.

bach et al. [25] investigated the effect of VC on the negative electrode, and reported that the addition of VC increases the cyclability and heat resistance and decreases the irreversible capacity by various analytical methods: cyclic voltammetry (CV), chronopotentiometry, impedance spectroscopy, FT–IR, X-ray photoelectron spectroscopy (XPS), electrochemical quartz crystal microbalance (EQCM). It was considered that the VC polymerizes on the lithiated graphite surfaces, and forms polyalkyl lithium-carbonate species that suppress both solvent and salt anion reduction [25]. Matsuoka et al. [26] studied the influence of VC on the decomposition of electrolyte solution and SEI formation on HOPG, and revealed that the VC deactivated reactive site on the HOPG and inhibits the furthermore decomposition of the electrolyte solution. Jeong et al. [27] investigated the effects of film-forming additives on HOPG in PC solutions by atomic force microscopy (AFM), and revealed that the thin SEI film precipitated in the presence of VC. The second purpose of the present paper is to investigate the role of VC on graphite electrode by the new impedance method developed for charge and discharge measurements. Although it was reported that VC brings about an effect to the stability of graphite electrode [25], there are also many unsolved problems such as a SEI formation mechanism.

The R_{sei} of the graphite electrode in 1 M $LiPF_6$–EC/EMC (3:7 by vol.) containing VC (2 wt.%) was determined by in situ EIS, where the experimental condition was the same as that in Fig. 4 except for the electrolyte solution. In the charge and discharge curves, the coulombic efficiency of delithiation during the first cycle was 93% and the irreversible capacity was 7%, indicating that the additive of VC into electrolyte solution reduces the irreversible capacity. The loci of the impedance spectra measured with the charge–discharge curves were similar to those without VC in Fig. 4. The plots of R_{sei} with and without VC against the capacity are shown in Fig. 7. In Fig. 7, the R_{sei} with VC (symbol (◆)) decreases remarkably in the initial period in the first cycle charge. Contrary to this, the R_{sei} without VC (symbol (▲)) increases in the initial period. This difference indicates that the addition of 2 wt.% VC forms the high quality SEI film at the early period of the first cycle charge. Furthermore, the values of R_{sei} with VC in the first cycle charge are smaller than that without VC, meaning that the presence of VC improves the permeation of lithium-ion in the SEI film. Aurbach et al. [25] also reported that R_{sei} of the impedance measured at constant potential decreases with the addition of VC. The results in Fig. 7 indicate the formation of thin and high density SEI film. In other words, comparing with the SEI film formed from the reduced materials of EC, the reduced materials of VC, which has double bond, generate the superior SEI film.

In Figs. 6 and 7, the R_{sei} shows the hysterisis during charge and discharge sequence. In order to discuss this hysterisis, the charge of graphite electrode under the condition in Fig. 6 was turned to discharge at 110 mAh g^{-1}. The R_{sei} during the discharge when the charge was turned at 110 mAh g^{-1} takes a small value and shows the hysterisis as same as the R_{sei} of full charge. These results indicate that the hysterisis originates from the direction of charge and discharge sequence. In the case of in situ EIS, since AC signal is superimposed on DC signal and the electrode is not under equilibrium, the intercalation (deintercalation) rate of lithium-ions is modulated during the charge (discharge). The permeation of lithium-ions in the SEI film involves not only migration but also solvation or desolvation step of

lithium-ions. Because the activation energy for desolvation of lithium-ion should be larger than that for the solvation, the R_{sei} for the intercalation during the charge is larger than R_{sei} for the deintercalation during the discharge.

4. Conclusions

The in situ electrochemical impedance spectroscopy in which the electrochemical impedance can be measured simultaneously with the charge and discharge of rechargeable batteries has been developed. Since it is unnecessary for this method to stop the charge and/or discharge, true impedance in the charge–discharge sequence can be measured directly by the in situ EIS. Furthermore, the in situ EIS has a great merit regarding the measurement time, namely, the electrochemical impedance spectra can be determined during the measurement of charge and discharge curves. It takes more than 30 min for one impedance spectrum from 10 mHz to 10 kHz, where this measurement time involves the time to attain the equilibrium at an arbitrary state of charge (capacity). If ten impedance spectra are measured by stopping the charge or discharge, the measurement time must increase more than 5 h.

By determining the resistances R_{sei} and R_{ct} for graphite electrode, the formation mechanism of SEI film and the intercalation mechanism were analyzed. Furthermore, the influence of the addition of VC into the electrolyte solution was investigated, and it has been clarified that the VC helps to form the high quality SEI film. This method is valid for not only negative electrode but also positive electrode and separator of lithium-ion rechargeable batteries. The authors believe that the investigations of the electrode reactions in various secondary batteries proceed by the present analytical method.

References

[1] R. Fong, U. von Sacken, J.R. Dahn, J. Electrochem. Soc. 137 (1990) 2009.
[2] R. Yazami, D. Guerard, J. Power Sources 43/44 (1993) 39.
[3] D. Aurbach, Y. Ein-Eli, B. Markovsky, A. Zaban, S. Luski, Y. Carmeli, H. Yamin, J. Electrochem. Soc. 142 (1995) 2882.
[4] J.O. Besenhard, M. Winter, J. Yang, W. Biberacher, J. Power Sources 54 (1995) 228.
[5] M. Inaba, Z. Siroma, A. Funabiki, Z. Ogumi, T. Abe, Y. Mizutani, M. Asano, Langmuir 12 (1996) 1535.
[6] M. Inaba, Z. Siroma, Y. Kawatate, A. Funabiki, Z. Ogumi, J. Power Sources 68 (1997) 221.
[7] M. Inaba, Y. Kawatate, A. Funabiki, S.K. Jeong, T. Abe, Z. Ogumi, Electrochemistry 67 (1999) 1153.
[8] M. Inaba, Y. Kawatate, A. Funabiki, S.K. Jeong, T. Abe, Z. Ogumi, Electrochim. Acta 45 (1999) 99.
[9] S. Zhang, M.S. Ding, K. Xu, J. Allen, T.R. Jow, Electrochem. Solid-State Lett. 4 (2001) A206.
[10] N. Takami, A. Satoh, M. Hara, T. Ohsaki, J. Electrochem. Soc. 142 (1995) 371.
[11] K. Chung, M.W. Chung, W.S. Kim, S.K. Kim, Y.E. Sung, Y.K. Choi, Bull. Korean Chem. Soc. 22 (2001) 189.
[12] C. Wang, A.J. Appleby, F.E. Little, Electrochim. Acta 46 (2001) 1793.
[13] T. Osaka, T. Momma, T. Tajima, Denki Kagaku 62 (1994) 350.
[14] Z.B. Stoynov, B.S. Savova-Stoynov, J. Electroanal. Chem. 183 (1985) 133.
[15] M. Itagaki, A. Taya, K. Watanabe, Electrochemistry 68 (2000) 596.
[16] Z.B. Stoynov, B.S. Savova-Stoynov, T. Kossev, J. Power Sources 30 (1990) 275.
[17] I. Epelboin, M. Keddam, J. Electrochem. Soc. 117 (1970) 1052.
[18] M. Itagaki, M. Tagaki, K. Watanabe, Electrochim. Acta 41 (1996) 1201.
[19] J.R. Dahn, Phys. Rev. B44 (1991) 9170.
[20] Z.X. Shu, R.S. McMillan, J.J. Murray, J. Electrochem. Soc. 140 (1993) 922.
[21] E. Peled, D. Golodnitsky, G. Ardel, J. Electrochem. Soc. 144 (1997) L208.
[22] D. Aurbach, A. Zaban, J. Appl. Electrochem. 348 (1993) 155.
[23] Y. Ein-Eli, Electrochem. Solid-State Lett. 2 (1999) 212.
[24] U. von Sacken, E. Nodwell, A. Sundher, J.R. Dahn, Solid State Ionics 69 (1994) 284.
[25] D. Aurbach, K. Gamolsky, B. Markovsky, Y. Gofer, M. Schmidt, U. Heider, Electrochim. Acta 47 (2002) 1423.
[26] O. Matsuoka, A. Hiwara, T. Omi, M. Toriida, T. Hayashi, C. Tanaka, Y. Saito, T. Ishida, H. Tan, S.S. Ono, S. Yamamoto, J. Power Sources 108 (2002) 128.
[27] S.K. Jeong, M. Inaba, R. Mogi, Y. Iriyama, T. Abe, Z. Ogumi, Langmuir 17 (2001) 8281.